Offshore loading facilities at Hay Point, Queensland

PART III

COASTAL STRUCTURES AND RELATED PROBLEMS

Green Island on the Great Barrier Reef

CHAPTER 107

SIMULTANEOUS WAVE AND CURRENT FORCES ON A PIPELINE

David A. Knoll, M.S., M.A.S.C.E.
Shell Oil Company
New Orleans, LA 7D16D

and

John B. Herbich, Ph.D., P.E., M.A.S.C.E.
Professor and Head, Ocean Engineering Program
Texas A&M University
College Station, TX 77843

INTRODUCTION

The hydrodynamic loads on an offshore pipeline resting on the ocean bottom are a function of parameters associated with waves and currents acting near the pipeline. There have been many studies conducted to develop the criteria needed to estimate the hydrodynamic loads imposed by waves and currents. Many of these studies have investigated the effect of these phenomena individually, but to date only limited research has been directed towards evaluating the combined effect. In general, the investigations of the interaction of waves and currents and their effect on the fluid force have been directed toward vertical piles[1,2,3,4,5] and structures in a random wave field with a current present;[6,7,8,9] however, the fluid force of waves in the presence of currents on pipelines has not been directly addressed.

The purpose of this research was to investigate the interaction of waves and currents and its relationship to the forces on submerged pipelines. A model pipeline in a wave-flume was used to obtain experimental values which were compared to values predicted by the Morison equation in conjunction with the superposition of the waves and a current.

The Morison equation[10] was used to evaluate the forces on a horizontal cylinder resting on the bottom. The two major input parameters required by this equation are (1) the water particle kinematics of velocity and acceleration; and (2) the coefficients of drag and inertia. The testing program investigated the drag forces developed by the combined waves and a current. The inertia forces were assumed small when compared to the drag forces since a relatively small diameter cylinder was used in the experiments, thus the accelerations were small.

The coefficient of drag was obtained directly by simultaneous measurements of the water particle kinematics and the fluid force on the cylinder. The horizontal velocity, predicted by Airy and Stokes third order wave theories in still water, was combined with a current by the algebraic addition of their respective horizontal velocity fields at a specific elevation. These velocities were compared directly to experimentally-determined values. Measured forces were then compared

to the forces obtained by the Morison equation, using the coefficients determined in this research and the kinematics of the modified Airy and Stokes third-order wave theories. The error associated with the algebraic addition assumption was investigated.

Many wave and current orientations are possible in the field, but only the case of a wave propagating in the direction of the current was investigated. It is felt that this orientation represents the most severe conditions that will be experienced in the field. Further investigations will be needed to verify this assumption. In order to develop the basic knowledge needed to understand the error associated with the superposition-principle assumption, the fundamental problem of mono-chromatic waves and currents must be evaluated before other effects such as random waves can be attempted.

The primary purpose of this research was not to develop explicit prototype design criteria, but to provide the design engineer with an insight into the parameters governing fluid force in combined wave and current conditions. The parameters for fluid force are affected by the interaction of waves and currents and the variation of these parameters are presented.

DATA ANALYSIS

The definition sketch of the idealized two-dimensional wave-current problem for offshore pipelines is given in Fig. 1. This

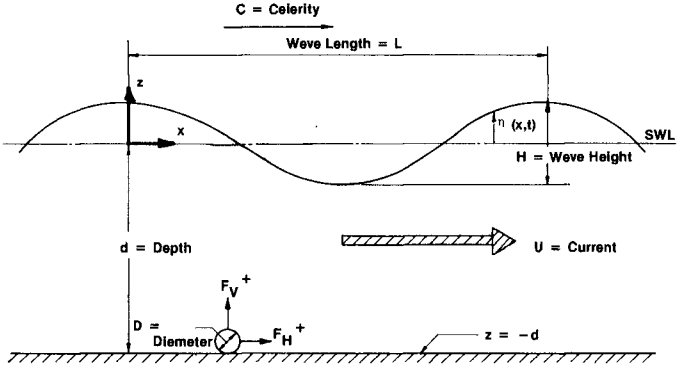

DEFINITION SKETCH OF THE PIPELINE PROBLEM

FIGURE 1

configuration may represent a pipeline resting on the ocean bottom. The cylinder has both horizontal and vertical forces acting on it due to the passing wave and current. Only the horizontal drag force is investigated in this research.

The Morison equation considers the total horizontal force (f_H) as the sum of the horizontal drag force (f_D) and the horizontal inertial force (f_I)(all forces expressed per unit length of cylinder):

$$f_H = f_D + f_I \quad \ldots \quad (1)$$

The drag force is a function of both a drag coefficient (C_D) and the horizontal component of the water particle velocity if the structure were absent (u), or:

$$f_D = \frac{C_D}{2} \rho D\, u|u| \quad \ldots \quad (2)$$

where D = diameter of cylinder
ρ = mass density of the fluid

The inertia force is a function of the inertial coefficient (C_I) and the horizontal particle acceleration (u), or:

$$f_I = C_I \frac{\rho \pi D^2}{4} \dot{u} \quad \ldots \quad (3)$$

Two of the major input parameters required by the Morison equation are the coefficients of drag and inertia. These coefficients must be determined experimentally. This is accomplished by measurements or theoretical predictions of the horizontal water particle kinematics in conjunction with fluid-force measurements. The coefficient of drag can be determined when the horizontal acceleration equals zero by the following equation:

$$C_D = \frac{2 f_D}{\rho D\, u|u|} \quad \ldots \quad (4)$$

when $f_I = 0$.

The coefficient of drag is generally presented as functions of two dimensionless parameters. The first parameter is the Reynolds number (N_{RE}). The Reynolds number indicates the dimensionless ratio of the inertial forces to the viscous forces in fluid motion, or:

$$N_{RE} = \frac{Du}{\nu} \quad \ldots \quad (5)$$

where D = characteristic length (diameter)
u = horizontal component of the particle velocity if the structure were absent at the time of interest
ν = kinematic viscosity

The second parameter, developed by Keulegan and Carpenter, is related to the coefficients of drag and inertia. This dimensionless parameter is also known as the "period parameter" and it relates the maximum amplitude of the oscillating particle velocity, including both wave and current (u_{max}), the period of the oscillatory motion (T) to the diameter of the cylinder (D):

$$N_{KC} = \frac{u_{max}T}{D} \quad \ldots\ldots\ldots\ldots\ldots\ldots\ldots\ldots \quad (6)$$

This parameter has been found to be related to the coefficients of drag and inertia for a very wide range of data.

The coefficient of drag determined experimentally in this research is presented as functions of these parameters.

Two other major input parameters required by the Morison equation are the particle kinematics of velocity and acceleration.

For a pipeline located near the ocean bottom, the water particle orbits are flattened (parallel to the bottom) for waves where the wave lengths are large compared to the water depth. The orbital motion changes to a horizontally oscillating flow when the water depth is small compared to the wave length; therefore, in this condition the variation of velocity over the height of the pipe is insignificant. This fact allows the velocity at the mid-point of the cylinder to represent the velocity used in the calculation of the fluid force by the Morison equation.

Airy and Stokes third-order wave theories are used in conjunction with the current to predict the combined flow field. In this case the parameters of wave height (H) and period (T) are considered to be the properties of a wave progressing in still water. These parameters are used with the water depth (d) to predict the velocities under a wave if no current were present. These resulting wave velocities are combined algebraically with the current velocity profile to predict the combined velocity profile. The equations and methods to determine the horizontal wave particle velocities predicted by Stokes third-order wave theory were those presented by Skjelbreia[11].

The effect of the viscous boundary layer of the wave was neglected in the calculation of the horizontal velocity near the bottom. Since the actual current velocity profile was used for superposition, the boundary layer due to the current was taken into account. Therefore, any error in the boundary layer was due to neglecting the boundary layer in velocity prediction of the wave theories.

The forces on submerged pipelines are related directly to the velocity field near the structure. Accurate prediction of the horizontal velocity fields is essential for the proper prediction of the forces on submerged pipelines. The error associated with the prediction of the combined horizontal velocity field is directly related to the error in the calculation of the horizontal force of a submerged pipeline.

EXPERIMENTAL METHODS AND EQUIPMENT

The experimental study was conducted in a two-dimensional wave-flume facility of the Ocean Engineering Program at Texas A&M University. The dimensions of the wave flume are 45.72 m (150 ft) in length, 0.46 m (1.5 ft) in width, and 1.22 m (4.0 ft) in depth. The test section was located approximately 18.29 m (60 ft) from the wave generator. Fig. 2 shows the general layout of the test facilities.

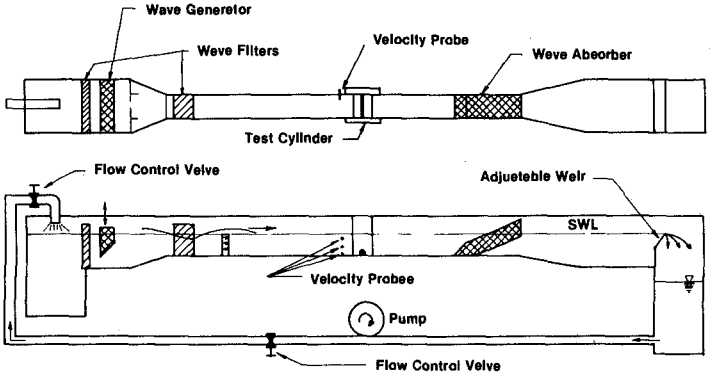

WAVE-CURRENT TEST FACILITY

FIGURE 2

The wave flume is constructed of a metal and wood frame, with one wall consisting of plywood and the other of plexiglass. Currents are produced by a pumping system capable of developing currents of 1.22 m/sec (4.0 ft/sec). The water depth for any specific flow rate was controlled by an adjustable weir located at the end of the tank.

A wave absorber was specially constructed for this investigation to reduce the reflection of the waves as shown in Fig. 3. The design permitted large volumes of water to be transmitted through the absorber so that significant currents could be produced.

The facilities included two measurement stations. Station one was for the measurement of surface parameters and water particle kinematics and station two was for fluid-force determination. Station one was used to gather the information for comparing the predicted water particle to the theoretical values. Station two was used to determine the fluid force on the test structure. Since the distance between the two stations is 1.26 m (4.13 ft), it is assumed that the wave characteristics do not change between the stations. Therefore, the results obtained at station one can be used at station two.

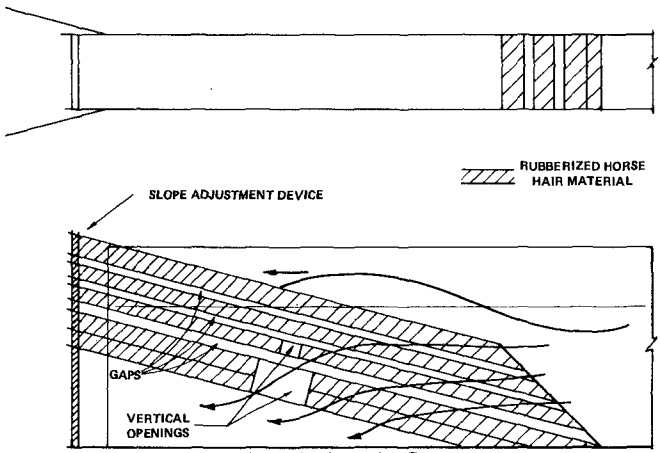

SCHEMATIC DIAGRAM OF CURRENT-PASSING WAVE ABSORBER

FIGURE 3

The test cylinder was constructed of polyvinyl chloride (PVC) pipe. Its outside diameter was 44.5 mm (1.75 in). The pipe was located 1.58 mm (.0625 in) above the bottom of the tank. This small gap provided for the free movement of the cylinder so that the unrestricted movement was transmitted to the load cell which converted this movement to an applied force. Since only horizontal components of force were being measured the effect of the gap was minimized. The test cylinder extended through the walls of the test tank. This extension helped to reduce end effects, which supported the two-dimensional assumption.

Measuring devices at station one consisted of a capacitance-type wave gauge and a hot-film anemometer probe as shown in Fig. 4. The capacitance-type wave gauge was used for surface profile measurements of wave height and period because of its availability and linearity. The results were recorded on a Hewlett Packard Model 74024 oscillographic strip recorder. This recorder was capable of providing a time reference on the recorded data. The period of the wave was determined by measuring the time between two successive wave crests. The capacitance-type wave gauge was used with a Hewlett Packard Model 17403A Carrier preamplifier. This preamplifier contained the full-bridge network required by the capacitance-type wave gauge. The output of the hot-film anemometer was amplified by a Hewlett Packard Model 17402A Low-Gain preamplifier before the output was recorded on the strip recorder.

A Thermo-Systems Model Series 1050 hot-film anemometer was used for the particle velocity measurements. This series consisted of a Model 1050A constant-temperature anemometer, a Model 1051 monitor and power supply, a Model 1055 linearizer, and a Model 1057 signal conditioner.

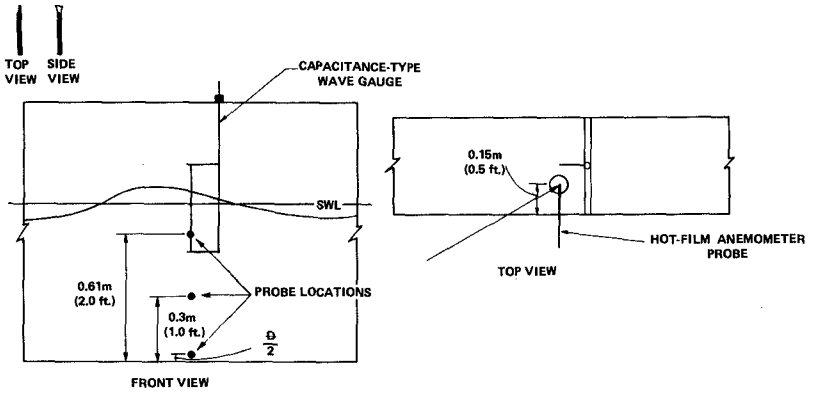

STATION ONE, SURFACE PROFILE AND VELOCITY MEASUREMENTS

FIGURE 4

The transducer used with the anemometer is a small resistance element which is heated and controlled at an elevated temperature. A Model 1210-20 hot-film transducer (probe) was used in this research. The amount of electrical energy dissipated in the sensor is a measure of the cooling effect of the fluid flowing past the heated sensor. The cooling effect of the fluid passing over the sensor depends on both the mass flow and temperature difference between the sensor and the fluid.

In operation, a current flows through the bridge. The amplifier senses any off balance, and feeds back more or less current until the bridge comes into balance. This additional electrical energy is outputted as a bridge voltage which is amplified and recorded on the oscillographic strip recorder.

It can be seen from Fig. 4 that three locations were used for water particle measurements. They were at 0.61 m (2.0 ft), 0.31 m (1.0 ft) and at the mid height of the cylinder at the bottom of the tank. The particle kinematics were compared at these elevations. The particle velocity at the mid height of the cylinder was used with the measured fluid force to determine the coefficient of drag. The probe was extended into one side of the tank a distance of 0.15 m (0.5 ft). This distance was selected so that the measured particle velocity would be out of the boundary layer, but the distance was short enough to reduce the effect of probe vibrations due to vortex shedding. The orientation of the probe in the fluid flow is important, because by aligning the probe perpendicular to the flow, only the horizontal component of the velocity is measured. The velocity parallel to the probe is not significant and can be assumed to be zero. With the orientation shown in

Fig. 4, only the horizontal velocity component was recorded. Only horizontal velocities and forces were investigated in this research.

Measurements at the second station consisted of a capacitance-type wave gauge and a mechanism to transmit the horizontal forces on a horizontal circular cylinder resting near the bottom to a load-cell device. A sketch of station two is shown in Fig. 5. The cylinder was connected

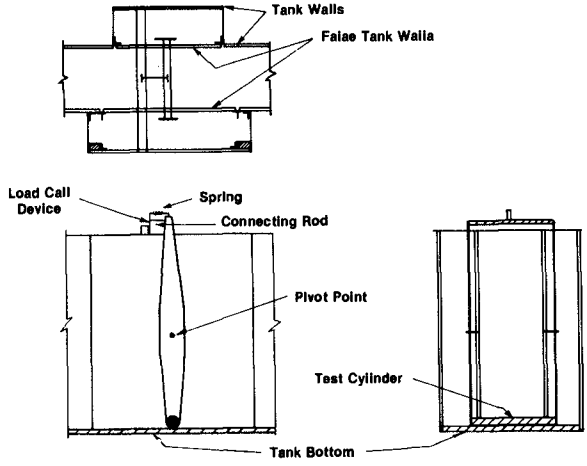

SCHEMATIC DIAGRAM OF STATION TWO, MODEL LOAD TEST STATION FIGURE 5

by two arms which rotated about a pivot point. This rotation transmitted the horizontal fluid force on the cylinder to a load cell located on the top of the tank. The load cell had a capacity of 1500 grams (≈3.0 lbs). The load cell was connected to the rotating mechanism by a rod which was pointed on both ends and which was held in place by a stiff spring. These pin-point connections were used to reduce friction. This total mechanism was capable of transmitting the positive or negative fluid force to the load cell without disrupting the fluid flow near the model. This device was found to be very effective in measuring the fluid force on the horizontal cylinder.

CALIBRATION AND PROCEDURE

All the equipment used in this investigation was calibrated using known values which were related to the output on the oscillograph recorder. All equipment was re-calibrated at each major test except for the hot-film anemometer which had to be calibrated periodically during the testing due to drift of the output.

The load cell was calibrated and balanced in a manner recommended by Hewlett-Packard. A known load was applied to the test cylinder, and

the output of the bridge network was recorded on the oscillograph recorder display. The applied load was transferred through a system of pulleys and weights described by the schematic diagram shown in Fig. 6.

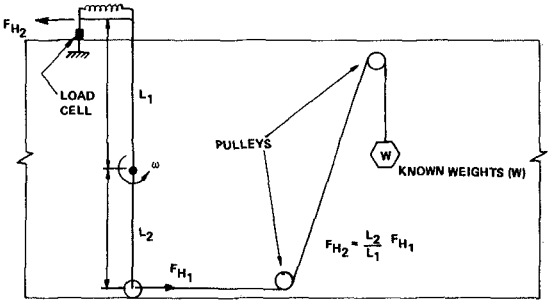

SCHEMATIC DIAGRAM OF LOAD-CELL CALIBRATION APPARATUS

FIGURE 6

The total force applied to the cylinder was equal to the suspended weight multiplied by the length ratio of the arms around the pivot point. Any losses due to friction were neglected. The known load was related to the output voltage recorded on the oscillography display by a linear ratio.

Calibration of the hot-film anemometer proved to be difficult, due to its non-linear output and the constant drift of the output voltage. The hot-film anemometer was calibrated by means of known velocities created by a forced pendulum. A schematic of the forced pendulum is shown in Fig. 7. The angular velocity (ω_1) of the driving mechanism is related to the velocity of the probe by the following equation:

$$V_p = \text{velocity of probe (ft/sec)} = 0.7857\ (\omega_1) \quad . \quad . \quad . \quad . \quad . \quad . \quad . \quad (7A)$$

$$V_p = \text{velocity of probe (m/sec)} = 0.2395\ (\omega_1) \quad . \quad . \quad . \quad . \quad . \quad . \quad . \quad (7B)$$

Four known velocities were used as calibration points for the hot-film anemometer. These velocities were measured using the same apparatus as the wave particle kinematics. The number of divisions for each calibration point was related to the velocity by fitting the data to a power curve.

An inherent problem of the hot-film anemometer is that the calibration will drift in a relatively short period of time. It was determined that significant drift occurred in a period of several hours. To

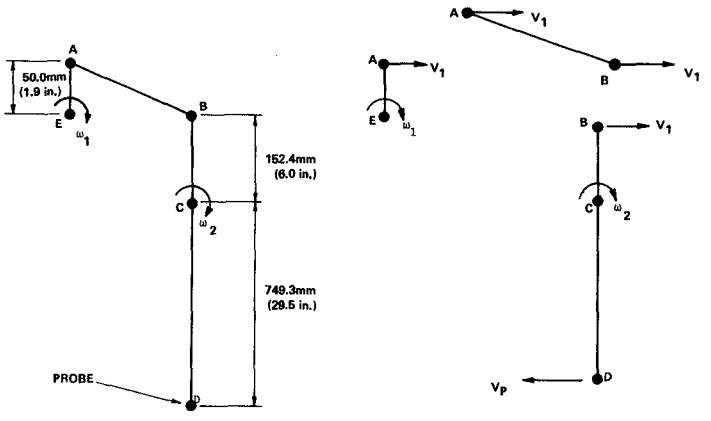

SCHEMATIC DIAGRAM OF THE FORCED PENDULUM FOR VELOCITY CALIBRATION

FIGURE 7

overcome this problem, the drift as a function of time was investigated. The drift was determined by running successive calibration tests during a period of one hour. The drift during the hour period was reasonably linear. Calibration tests were run periodically during the test periods. This procedure proved successful for calibrating the hot-film anemometer.

The testing program was divided into two major stages. One stage was the determination of the water particle kinematics at three elevations with the wave surface parameters; the other was the measurement of the simultaneous fluid-force measurements and particle kinematics measurements required to determine the coefficient of drag.

All data were recorded on the oscillograph recorder and digitized and then used as input for a computer program which fitted the velocity data to a power curve. This program then wrote the calibrated data and other parameters of the particular test to a computer data file, where it was stored for computer analysis.

DATA ANALYSIS AND RESULTS

The results obtained from the testing program were based on several assumptions. First, the wave reflections from the sides and end of the wave tank were considered to have very little effect on the measurements. Secondly, the flow was assumed to be essentially two-dimensional. This was supported by the fact that the aspect ratio of the model was 10.274. Thirdly, the flow was considered irrotational, and the fluid was

inviscid. This assumption, which is vital for the validity of the superposition principle, has been found to be incorrect for currents with a varying velocity profile. The quantification of the error associated with this assumption was the basic goal of the research.

The thrust of the data analysis was two-fold. One task was to determine the error associated with the superposition of the current velocity field and the velocity field generated by a wave propagating in still water. This was accomplished by directly measuring the error over a specific range of waves and currents. The velocity field of the waves was predicted by both Airy and Stokes third-order wave theories.

The other task was a comparison of the measured forces on the pipeline model with the forces predicted by this superposition principle. The experimental drag coefficients were determined by simultaneous measurements of horizontal fluid velocity and fluid force. Comparisons were then made to the coefficients determined from the superposition principle using Airy or Stokes third-order wave theories.

For the first task, kinematic measurements were taken at three elevations as discussed previously. The second task employed a fourth test to measure forces on the model pipeline. The range of wave parameters and currents tested are presented non-dimensionally in Table 1. Since tests Nos. 3 and 4 were conducted simultaneously, the range of values for both tests were identical.

TABLE 1

RANGES OF WAVE AND CURRENT PARAMETERS FOR TESTING PROGRAM

TEST	$\frac{H}{d}$	$\frac{H}{gT^2}$	$\frac{d}{gT^2}$	$\frac{U}{u}$	$\frac{H}{L}$
1. HORIZONTAL PARTICLE VELOCITY MEASUREMENT ELEVATION = 0.61 M (2.0 FT.)	0.1358-0.291803	0.0415-0.0230	0.0639-0.1102	0.1439-1.0179	.09896-.09186
2. HORIZONTAL PARTICLE VELOCITY MEASUREMENT ELEVATION = 0.30 M (1.0 FT.)	0.1715-0.2912	0.0107-0.0238	0.0551-0.1253	0.0000-5.3316	.07265-.12429
3. HORIZONTAL PARTICLE VELOCITY MEASUREMENT ELEVATION = 0.02 M (0.145 FT.)	0.1155-0.2407	0.0128-0.0197	0.0563-0.1155	0.0000-4.9602	.08699-.12508
4. HORIZONTAL FORCE MEASUREMENT	0.1155-0.2407	0.0128-0.0197	0.0563-0.1155	0.0000-4.9602	.08699-.12508

The raw data for tests Nos. 1-3 consisted of wave heights, wave periods, and a continuous measurement of horizontal fluid velocity over the wave period. The raw data for test No. 4 included a continuous record of horizontal fluid force over the period. The estimated error associated with each of these input variables is presented in Table 2.

TABLE 2

ESTIMATED ACCURACY OF EXPERIMENTAL MEASUREMENTS

VARIABLE	MAXIMUM ERROR	MAJOR SOURCE OF ERROR
WAVE HEIGHT	2 TO 5 PERCENT	STABILITY AND LINEARITY OF BRIDGE NETWORK AND RECORDING DEVICE; WAVE REFLECTION
WAVE PERIOD	± .05 SECONDS	DETERMINATION OF WAVE CREST FROM RECORDING DEVICE
WATER DEPTH	6 MM (.25 IN.)	VARYING WATER DEPTH DUE TO CURRENT
FLUID FORCE	2 TO 3 PERCENT	DETERMINATION FROM RECORDED OUTPUT; STABILITY AND LINEARITY OF BRIDGE NETWORK
FLUID VELOCITY	1 TO 8 PERCENT	CALIBRATION AND DRIFT OF HOT-FILM ANEMOMETER (THIS ERROR IS GREATEST AT LOW VELOCITY DUE TO CURVE FIT PROCESS OF OUTPUT VOLTAGE TO VELOCITY)

The largest error was associated with the fluid velocity measurements of the hot-film anemometer. The error reached its maximum at the lower velocities, which were not within the range of the calibration curves.

The relative error of the superposition principle of the horizontal velocities can be expressed as a dimensionless difference (E):

$$E = \frac{u_{mea} - u_{tot}}{\frac{\pi H}{T}} \quad \ldots\ldots\ldots\ldots\ldots\ldots\ldots\ldots (8)$$

where u_{mea} = the measured horizontal velocity at elevation (z),
u_{tot} = the algebraic sum of the horizontal particle velocity at elevation (z) predicted by either Airy or Stokes third order wave theory and the current velocity,
H = wave height, and
T = wave period.

Dividing by the Airy deepwater horizontal velocity at the still water elevation the difference was non-dimensionalized.

The dimensionless difference (E) was found to be a function of a dimensionless parameter (R) relating the magnitude of current to the horizontal particle velocity of the wave in still water:

$$R = \frac{U}{u_{calc}} \quad \ldots\ldots\ldots\ldots\ldots\ldots\ldots\ldots\ldots\ldots \quad (9)$$

where U = current velocity at elevation (z),
u_{calc} = horizontal particle velocity predicted by either Airy or Stokes third order wave theories in the absence of a current at elevation (z).

The relationship between the dimensionless difference (E) and the velocity ratio (R) for an elevation of 1.0 ft above the bottom under the wave crest is shown in Fig. 8 for Airy wave theory and Fig. 9 for Stokes third-order wave theory.

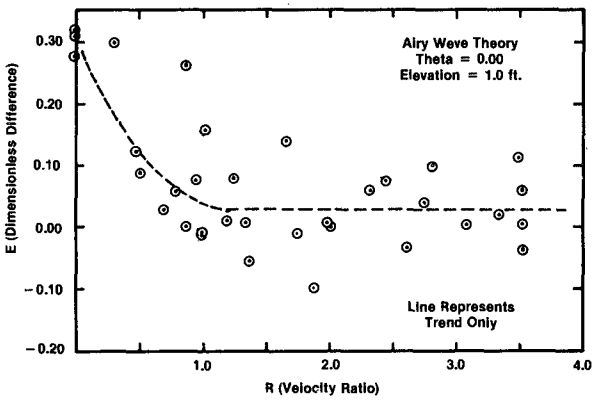

DIMENSIONLESS DIFFERENCE VERSUS THE VELOCITY RATIO FOR AIRY WAVE THEORY AT ELEVATION 1.00 FT (THETA = 0.00)

FIGURE 8

Several interesting results can be noted from these figures. The wave theories tend to under-predict (positive dimensionless difference) the horizontal velocity at elevation (z) when no current is present (R = 0.0). As the current velocity increased relative to the wave particle velocity, the error decreased to approximately zero for values of R > 1.0. This trend is represented by the dotted lines on each of the figures. This trend seems to indicate that the superposition of the velocity fields approaches reasonable agreement with the measured values for R > 1.0.

A slight tendency exists for Stokes third-order wave theory to predict the superimposed velocity superior to that of Airy prediction. This can be seen by the mean error which is closer to the zero error line.

The fluid force data were analyzed at the crest to determine the drag coefficient. At this point the acceleration is equal to zero and

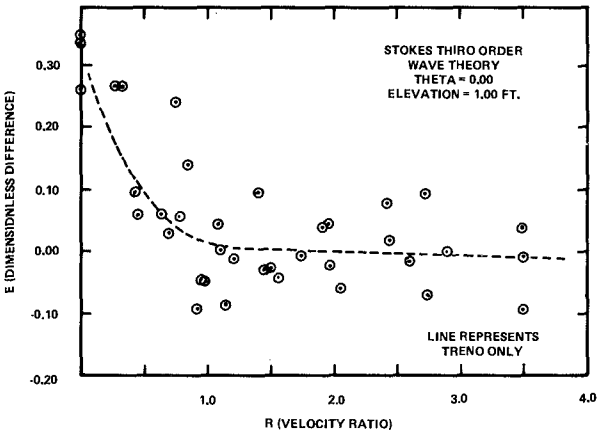

DIMENSIONLESS DIFFERENCE VERSUS VELOCITY RATIO FOR STOKES THIRD ORDER WAVE THEORY AT ELEVATION 1.00 FT. (THETA = 0.00)

FIGURE 9

only the drag force is present. The coefficients of drag were determined by three methods. The first method used simultaneous measurements of the horizontal fluid force and velocity.

The second and third methods were based on the predicted velocities of the superposition principle using Airy and Stokes third-order wave theories to calculate the coefficient of drag. A comparison of the three methods was made to demonstrate the differences in the coefficient of drag.

The coefficient of drag is related to the Reynolds Number (N_R). The coefficient of drag was plotted as a function of the Reynolds number in Fig. 10 as computed by the simultaneous measurements of fluid force and fluid velocity; Fig. 11 as computed using the superposition principle with Airy wave theory; and Fig. 12 as computed using Stokes third-order wave theory.

These figures all show the same general trend of reduction in the coefficient of drag with increasing Reynolds numbers.

Figures 10 and 11 show that the coefficient of drag was less when computed from the measured velocity as opposed to the Airy or Stokes III velocities for the range of Reynolds numbers shown. This is related to the fact that the wave theories used in conjunction with the superposition principle have a tendency to under-predict the horizontal velocity near the bottom boundary.

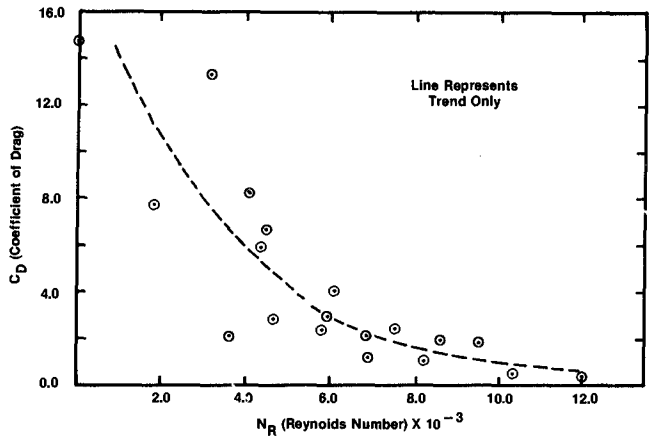

COEFFICIENT OF DRAG VERSUS REYNOLDS NUMBER FROM SIMULTANEOUS FORCE AND VELOCITY MEASUREMENTS

FIGURE 10

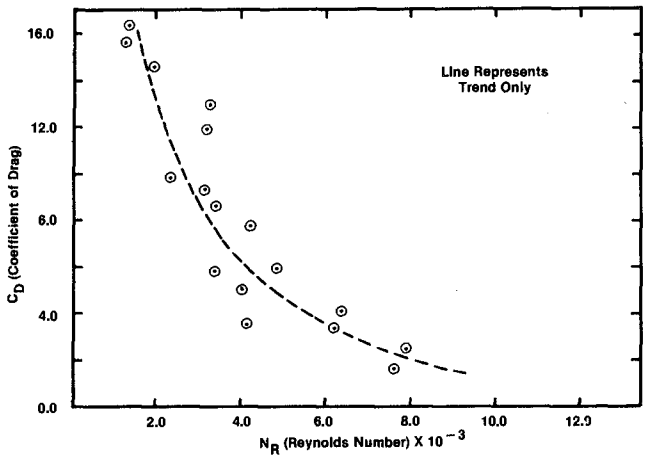

COEFFICIENT OF DRAG VERSUS REYNOLDS NUMBER FROM COMPUTATIONS USING AIRY WAVE THEORY

FIGURE 11

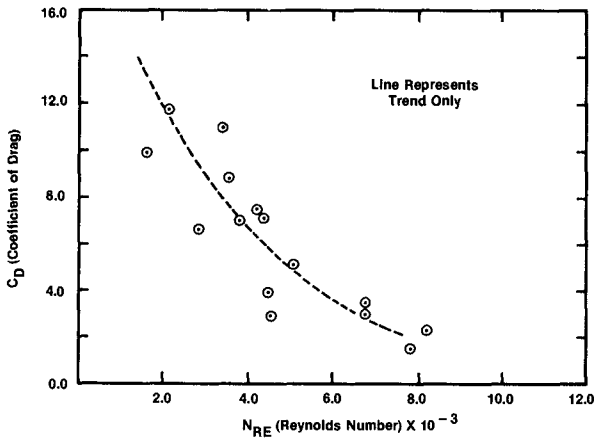

COEFFICIENT OF DRAG VERSUS REYNOLDS NUMBER FROM COMPUTATIONS USING STOKES THIRD ORDER WAVE THEORY

FIGURE 12

The relative difference between the coefficients of drag computed by Airy wave theory and those computed from measured values are shown in Fig. 13. This figure demonstrates at low velocity ratios (R) the coefficients computed using Airy wave theory are greater than the actual values, but this difference decreases with increasing currents.

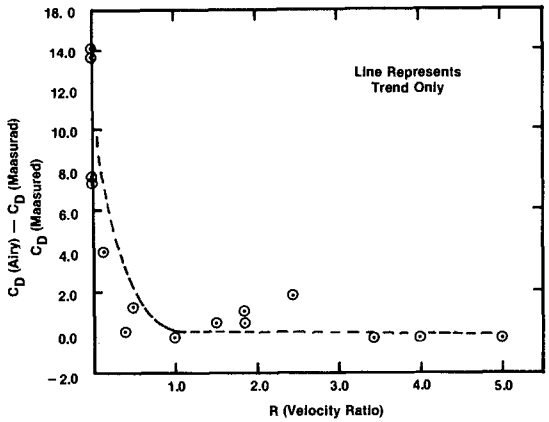

RELATIVE DIFFERENCE OF C_D FOR AIRY WAVE THEORY AND MEASURED VALUES VERSUS THE VELOCITY RATIO

FIGURE 13

The coefficients of drag computed by the simultaneous measurements of the horizontal fluid force and velocity are, by definition, the actual values. These coefficients can only be used if the actual horizontal velocity can be predicted. This supports the fact that the coefficients of drag are dependent on the method used to determine the horizontal velocity. Therefore, the prediction of forces on a cylinder should be consistent with the method which was used to determine the coefficients.

For the steady-state current condition, Fig. 14 shows the actual coefficient of drag for the horizontal cylinder.

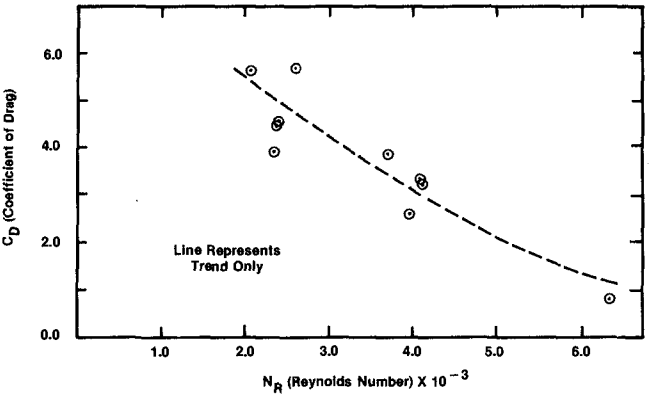

COEFFICIENT OF DRAG VERSUS REYNOLDS NUMBER (STEADY-STATE CURRENT CONDITION)

FIGURE 14

The primary purpose of this research was to determine the drag forces associated with the horizontal velocity. The drag forces were determined when the velocity was maximum and the acceleration was zero. Therefore, no inertial effects were present and the coefficient of drag was unaltered by this effect.

CONCLUSIONS AND RECOMMENDATIONS

The following conclusions were evident from the testing program for the range of values tested.

1. Airy and Stokes third-order wave theories in conjunction with the superposition principle predict the horizontal velocity reasonably well for velocity ratios ($R = \frac{U}{u}$) greater than one. The velocities are under-predicted for u values of R less than one.

2. The coefficients of drag computed from Airy and Stokes third order wave theories in conjunction with the superposition principle are greater in magnitude than the values determined by the simultaneous force and velocity measurement. This difference decreases with increasing velocity ratios.

The conclusions were based on a limited testing program. These results can be extended over a greater range of waves and currents by further tests. These additional tests will indicate whether any scale effects are important.

Other conditions related to the pipeline problem, such as the distance of the cylinder from the boundary, the transverse (lift) force, relative roughness and orientation angles, should be investigated for the combined wave-current condition.

Other theories developed for the interaction of waves and currents should be tested experimentally to determine their accuracy for the prediction of fluid force and particle kinematics.

REFERENCES

1. Dalrymple, Robert A., "Models for Nonlinear Water Waves on Shear Currents," Offshore Technology Conference, 1974, Paper No. 2114.
2. Dalrymple, Robert A., "Waves and Wave Forces in the Presence of Currents," Civil Engineering in the Oceans, 1970, Vol. 2, pp. 999-1018.
3. Davis, D. A. and Ciani, J. B., "Wave Forces on Submerged Pipelines - A Review with Design Aids," Naval Facilities Engineering Command, Technical Report No. R844, July 1976, 55 pages.
4. Dean, R. G., "Stream Function Representation of Nonlinear Ocean Waves," Journal of Geophysical Research, Vol. 70, No. 18, September 15, 1965.
5. Garrison, C. J. and Rao, U. S., "Interaction of Waves With Submerged Objects," Journal of the Waterways, Harbors and Coastal Engineering Division, American Society of Civil Engineers, Vol. 97, No. WW2, May 1971, pp. 259-277.
6. Tung, Chi Chao and Huang, Norden E., "Combined Effects of Currents and Waves on Fluid Force," Ocean Engineering, Vol. 2, No. 4, 1973, pp 183-193.
7. Tung, Chi Chao and Huang, Norden E., "Influence of Wave-Current Interactions on Fluid Force," Ocean Engineering, Vol. 2, No. 5, 1973, pp 207-218.
8. Tung, Chi Chao and Huang, Norden E., "Influence of Current on Statistical Properties of Waves," Journal of the Waterways, Harbors and Coastal Engineering Division, Vol. 100, 1974, pp. 267-278.
9. Wu, Song C. and Tung, Chi Chao, "Structural Response to Wave and Current Forces," Civil Engineering in the Oceans, Vol. 2, 1975, pp. 849-864.
10. Morison, J. R., O'Brien, M. P., Johnson, J. W. and Schaaf, S. A., "The Force Exerted by Surface Waves on Piles," Petroleum Transactions, American Institute of Mining, Metallurgical, and Petroleum Engineering, Vol. 189, 1950, pp. 149-154.

11. Skjelbreia, Lars, "Gravity Waves: Stokes Third Order Approximation, Tables of Functions," Council on Wave Research, The Engineering Foundation, 1959, p. 336.